ARCHIVES OF ELECTRICAL ENGINEERING VOL. 72(4), pp. 895–913 (2023)

DOI 10.24425/aee.2023.147417

Core loss resistance impact on sensorless speed control of an induction motor using hybrid adaptive sliding mode observer

TADELE AYANA, LELISA WOGI, MARCIN MORAWIEC ✉

Faculty of Electrical and Control Engineering, Gdansk University of Technology
Gabriela Narutowicza 11/12, 80-233 Gdansk, Poland
e-mail: {tadele.ayana/lelisa.wogi/✉marcin.morawiec}@pg.edu.pl

(Received: 10.04.2023, revised: 04.07.2023)

Abstract: Induction motors (IMs) experience power losses when a portion of the input power is converted to heat instead of driving the load. The combined effect of copper losses, core losses, and mechanical losses results in IM power losses. Unfortunately, the core losses in the motor, which have a considerable impact on its energy efficiency, are not taken into account by the generally employed dynamic model in the majority of the studies. Due to this, the motor rating often corresponds to the worst-case load in applications, but the motor frequently operates below rated conditions. A hybridized model reference adaptive system (MRAS) with sliding mode control (SMC) is used in this study for sensorless speed control of an induction motor with core loss, allowing the motor to operate under a variety of load conditions. As a result, the machine can run at maximum efficiency while carrying its rated load. By adjusting the α-axis current in the $\alpha - \beta$ reference frame in vector-controlled drives, the system's performance is enhanced by running the motor at its optimum flux. Regarding the torque and speed of both induction motors with and without core loss, the Adaptive Observer Sliding Mode Control (AOSMC) has been constructed and simulated in this case. The AOSMC with core loss produced good performance when the proposed controller was tested.

Key words: induction motor, loss minimization, core loss, adaptive observer, sliding mode controller

Nomenclature

"^"	is the estimated value,
R_s, R_r	are the stator and rotor resistances,
L_s, L_r	are the stator and rotor inductances,

R_m, L_m	are the core resistance and magnetizing inductance,
J, T_L	are the inertia and load torque,
$i_{s\alpha,\beta}$, $i_{m\alpha,\beta}$	are the vector components of stator and magnetizing currents,
$v_{s\alpha,\beta}$	is the vector components of stator voltages,
ω_r, Te	are the rotor angular speed and electromechanical torque,
$\psi_{r\alpha,\beta}$, $\psi_{m\alpha,\beta}$	are the rotor and magnet flux components,
p	is the number of pole pairs,
ω_r^*	is the reference speed.

1. Introduction

Due to their straightforward mechanical design, low maintenance needs, and reduced cost compared to the similarly prevalent DC motors in industry, induction motors are widely utilized in industrial applications.

Scalar and vector control approaches have been extensively employed in the past ten years when investigating various induction motor control systems. Scalar control is frequently employed for low-performance applications. These traditional control methods involve applying nonlinear transformations, feedback, and PI control loops to the vector velocity and rotor flux modules in order to asymptotically decouple them. With different control approaches, IM performance has lately improved. Artificial neural networks, adaptive backstepping, sliding mode, and adaptive input-output linearization are only a few of the topics under active development. Yet it is important to note that the majority of them as well as the references therein are based on a mathematical induction motor model that ignores power core losses, indicating that the induction motor performs inefficiently. The power core losses must be taken into account if high efficiency performance is required, and the control law must be designed under the conditions acquired by reducing the power core losses.

Induction motor design optimization relies on the choice of independent variables, if numerous variables are employed, optimization becomes difficult. Variable selection is therefore essential for optimizing motor designs. An example of a common nonlinear programming problem is shown in the following, identifying a large set of motor variables that can be decreased or maximized depending on the desired reduction in complexity or improvement in performance [1–5].

Since induction motors are the primary users of electric energy in industry, this problem has grown in importance as a matter of study over the past two decades. As a result, efforts are being made to increase IM efficiency, which is also a current active research topic.

The model uses sliding mode control (SMC), adaptive control, and artificial intelligence (AI) techniques for high-performance applications. The key characteristic of SMC is that it performs well dynamically throughout a broad range of non-linearity, is unaffected by parameter variation, and brings the dynamic system relatively close to the specified sliding surface. However, the chattering of discontinuous functions such as switching time delay, small-time constant, and high switching frequency is not eliminated by conventional SMC [6].

The immeasurable induction motor parameters are significant to control system designers since none of the state variables of the induction motor are quantifiable. To overcome such difficulties, observers, estimators, and filters are used. It is common practice to forecast the im-

measurable parameters from the measurable stator voltage and current using full-order observers and reduced-order observers.

In [7] vector control and adaptation are used to get rid of speed-dependent characteristics and create a stable control system. The command signal is produced by the author utilizing a field-oriented control system and a traditional PI fixed gain tuner.

Model-based approaches depend on motor characteristics since they use models to estimate losses and subsequently minimize them. They fit the following definition: To achieve lowest-loss operation, a model-based LMT relies on motor characteristics and a power-loss or input power model. Although it may use other feedback, it does not contain closed-loop power measurement or estimation [8].

It has been determined that the Siding Mode Control Observer (SMO) is an effective way to increase the speed observer's resilience [9–11]. Unfortunately, there is a chattering problem as a result of the high-frequency switching control. It has therefore become a crucial area for SMO improvement through chatter suppression. Initially, methods for the integral SMO based on boundary layers have been described [12, 13]. To quiet the noise, they primarily impair the system's resilience and there is the steady-state error problem with system disturbance [14].

In [10], a second-order SMO based on SMC's field-oriented control was suggested. Theoretically, chattering can be eliminated by putting the high-frequency switching control in its derivatives. The steady-state error problem is then resolved [15] by forcing the sliding-mode state and its first derivative to equal zero in a certain amount of time. The super twisting high order is a tool for chattering attenuation and has been used to predict mechanical and rotor position speeds as well as track parameter alterations online [16–19].

Utilizing an adaptive observer and sliding mode control, induction motor direct torque control is improved [20], but core loss is not included.

The fundamental dynamic model is used in many studies to simulate the performance of the motor and apply new controls. For instance, in [21], the traditional model is utilized to calculate the parameters and performance factors using data from the motor manufacturer. The influence of the core losses is not depicted in the model hence, the results may not be accurate.

The same problem is present in [22], which builds a simulation file for an induction motor supplied using the same model without core losses. If that is the case, there is a deficit in the simulated input power, which omits core losses and provides erroneous efficiency values.

Two sorts of motor efficiency-improving control strategies exist: a loss model-based controller (LMC) and a search controller (SC). The fundamental workings of the search controller are as follows: for a given torque and speed, measure the input power, and then repeatedly look for the flux level (or its equivalent variables) until the least input power is found [23]. The delayed convergence and torque ripples of the search controller are significant flaws.

The model-based controller uses the machine model to calculate losses before choosing a flux level to reduce them [24, 25]. LMC moves quickly and without torque ripple. The precision, though, is dependent on accurate modelling of the motor drive and losses. In this study, the induction motor is modelled taking core loss resistance into account, an advanced hybridized control mechanism, namely the AOSMC, is designed, and its performance is checked by simulations for different load conditions and stability.

2. Modeling of induction motor with core loss

The iron loss of a motor is related to core structure parameters, voltage and frequency, and flux density. If the motor's iron loss is taken into account in the dynamic model, the loss of an equivalent pure resistance winding can be used to depict the motor's iron loss. The corresponding winding of the stator is only assumed on the stator because the stator iron loss is typically the primary component in asynchronous motors. Apart from the four windings on the original stator and rotor axes, two equivalent iron loss windings are added to the stator side in the $(\alpha\beta)$ stationary coordinate system.

The voltage equations are written as [26]

$$\begin{aligned} v_{s\alpha} &= R_s i_{s\alpha} + \frac{\mathrm{d}\psi_{s\alpha}}{\mathrm{d}t}\,, \\ v_{s\beta} &= R_s i_{s\beta} + \frac{\mathrm{d}\psi_{s\beta}}{\mathrm{d}t}\,, \\ 0 &= R_r i_{r\alpha} + \omega_r \psi_{r\beta} + \frac{\mathrm{d}\psi_{r\alpha}}{\mathrm{d}t}\,, \\ 0 &= R_r i_{r\beta} - \omega_r \psi_{r\alpha} + \frac{\mathrm{d}\psi_{r\beta}}{\mathrm{d}t}\,, \\ 0 &= R_m i_{Rm\alpha} - \frac{\mathrm{d}\psi_{m\alpha}}{\mathrm{d}t}\,, \\ 0 &= R_m i_{Rm\beta} - \frac{\mathrm{d}\psi_{m\beta}}{\mathrm{d}t}\,, \end{aligned} \tag{1}$$

where: $i_{Rm\alpha}$ and $i_{Rm\beta}$ are the equivalent iron loss resistance currents on the α-axes and β-axes, $i_{r\alpha}$ and $i_{r\beta}$ are the α-axes and β-rotor currents, $\psi_{s\alpha}$ and $\psi_{s\beta}$ are the stator fluxes.

The relationships between magnetic fluxes and currents are as follows:

$$\begin{aligned} \psi_{s\alpha} &= L_s i_{s\alpha} + \psi_{m\alpha}\,, \\ \psi_{s\beta} &= L_s i_{s\beta} + \psi_{m\beta}\,, \\ \psi_{r\alpha} &= L_r i_{r\alpha} + \psi_{m\alpha}\,, \\ \psi_{r\beta} &= L_r i_{r\beta} + \psi_{m\beta}\,, \\ \psi_{m\alpha} &= L_m i_{Lm\alpha}\,, \\ \psi_{m\beta} &= L_m i_{Lm\beta}\,, \end{aligned} \tag{2}$$

where $i_{Lm\alpha}$ and $i_{Lm\beta}$ are the α-axes and β-axes excitation currents.

The motor excitation current equations are given as,

$$\begin{aligned} i_{Lm\alpha} &= i_{s\alpha} + i_{r\alpha} - i_{Rm\alpha}\,, \\ i_{Lm\beta} &= i_{s\beta} + i_{r\beta} - i_{Rm\beta}\,. \end{aligned} \tag{3}$$

The torque equation is given as

$$T_e = \frac{L_m}{L_r}\left(\psi_{r\alpha}\left(i_{s\beta} - i_{Rm\beta}\right) - \psi_{r\beta}\left(i_{s\alpha} - i_{Rm\alpha}\right)\right). \tag{4}$$

The equation of motion is given as

$$\frac{\mathrm{d}\omega_r}{\mathrm{d}t} = \frac{p}{j}\left(T_e - T_l\right). \tag{5}$$

The dynamic mathematical model of an asynchronous motor considering iron loss in stationary coordinates can be composed from Eqs. (1) to (5) and the equivalent circuit as shown in Fig. 1.

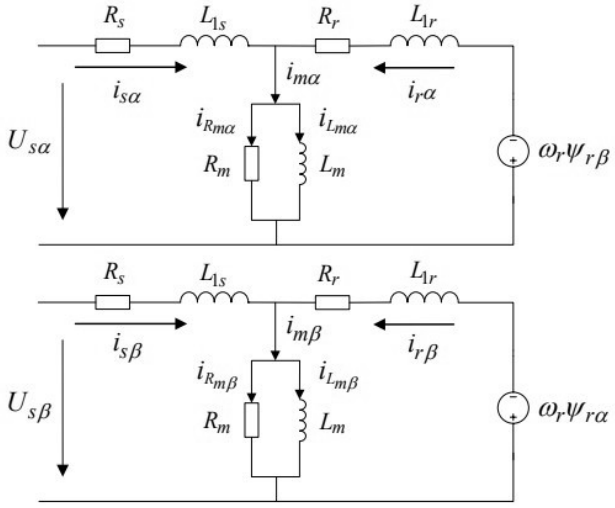

Fig. 1. The equivalent circuit of asynchronous motor considering iron loss in stationary coordinate system [26]

From Fig. 1, it is possible to drive the equation for the stator leakage inductance L_{1s} and rotor leakage inductances L_{1r} as,

$$\begin{aligned} L_{1s} &= L_s - L_m\,, \\ L_{1r} &= L_r - L_m\,. \end{aligned} \tag{6}$$

3. Design of the proposed controller

Both linear and nonlinear systems have used sliding mode control (SMC). As an adaptive observer, a sliding mode control with a variable control structure is used, which provides the drive system with good performance with parameter variation and load torque disturbance. The driving response is pushed to track or slide the predetermined sliding surface according to the SMC concept. In order to build the state observer and follow the drive system's response to the reference model signal, sliding mode control (SMC) was used [27].

The scalar equation [28] establishes the sliding surface's state space definition as

$$s\left(e,\, \dot{e},\, t\right), \tag{7}$$

where s stands for sliding as the function of error e, rate of change of error $\dot{e}$ and time t.

The sliding variable s is

$$s = \dot{e} + \lambda e, \tag{8}$$

where λ relies on the system's bandwidth and is a positive constant.

Tracking is similar to staying permanently on the sliding surface, and the sliding variable s is kept at zero.

The condition of sliding mode is

$$\frac{1}{2}\frac{\mathrm{d}s^2}{\mathrm{d}t} = \eta|s|, \tag{9}$$

where η is a strictly positive design constant.

Sliding mode control (SMC) is used to establish the state observer and monitor the drive system's response to the reference model signal. The primary focus of the sliding surface design was the driving system's reachability requirement.

The goal of the control strategy is to get the motor speed to follow a given time-varying instruction despite model uncertainty, load torque fluctuations, and measurement noise. With sliding mode control, the system is managed so that the tracking error (e) and its rate of change are constantly moving in the direction of a sliding surface.

$$e = \omega_r - \omega_r^* . \tag{10}$$

3.1. Observer design

The observer model used for the MRAC system is based on the state-space model of the induction motor at the stationary reference frame.

The linear time-invariant system can be expressed as

$$\begin{aligned} \frac{\mathrm{d}x}{\mathrm{d}t} &= \boldsymbol{A}x + \boldsymbol{B}u, \\ y &= \boldsymbol{C}x. \end{aligned} \tag{11}$$

where: $\boldsymbol{A}$ represents the state matrices, $\boldsymbol{B}$ represents the input matrices, $\boldsymbol{C}$ and x is the state variable and moreover given by

$$x = \begin{bmatrix} i_{s\alpha} & i_{s\beta} & \psi_{r\alpha} & \psi_{r\beta} & i_{m\alpha} & i_{m\beta} & \omega_r \end{bmatrix}^T, \tag{12}$$

where T is the matrix transpose.

The extended speed observer model is written as

$$\begin{aligned} \hat{x}_e &= \boldsymbol{A}_e\hat{x}_e + \boldsymbol{B}_e u, \\ \hat{y}_e &= \boldsymbol{C}_e\hat{x}_e , \end{aligned} \tag{13}$$

where: $\hat{x}_e = [\hat{i}_{s\alpha} \;\; \hat{i}_{s\beta} \;\; \hat{\psi}_{r\alpha} \;\; \hat{\psi}_{r\beta} \;\; \hat{i}_{m\alpha} \;\; \hat{i}_{m\beta} \;\; \hat{\omega}_r]^T$ represents the state vector variables, $u = [u_{s\alpha} \;\; u_{s\beta}]^T$ represents the input vectors and $\boldsymbol{A}_e, \boldsymbol{B}_e, \boldsymbol{C}_e$ are the system's parameter matrices.

The error dynamics of the system is

$$\hat{x}_e = \boldsymbol{A}_e\hat{x}_e + \boldsymbol{B}_e u + k(y - \hat{y}_e), \tag{14}$$

where k ($k_1 = 0.006$, $k_2 = 0.01$, $k_3 = 0.8$, $k_4 = 0.5$) are the observer tuning gains.

The next stage is to choose what are known as switching functions, the sliding mode system's goal is to ensure that these functions have a zero value.

In the context of estimator applications, the switching function forms are typically where estimating errors occur. In the instance of induction motor speed estimate, it will be shown that they can also be a combination of state variables and estimation errors [29].

They can be written as in the following vector:

$$s = [s_1 \;\; s_2 \;\; s_3 \;\; \ldots \;\; s_n]^T, \tag{15}$$

where the size of the vector matches the largest dimension of the vector of control signal in the system design.

The switching functions vector's derivative must be understood for the design process as

$$\dot{s} = [\dot{s}_1 \;\; \dot{s}_2 \;\; \ldots \;\; \dot{s}_n]^T. \tag{16}$$

It is necessary to select the switching functions vector (15) in a way that enables the decomposition of (16) which is represented by the following equation:

$$\dot{s} = \boldsymbol{f} + \boldsymbol{d}k, \tag{17}$$

where $\boldsymbol{d}$ is the matrix that depends on the vector of the control signal k and $\boldsymbol{f}$ is the column vector that is independent of k. In addition, the vector $\boldsymbol{f}$ can be broken down into:

$$\boldsymbol{f} = f_1 + f_2, \tag{18}$$

where f_1 is the portion that can be determined using signals that have been measured or estimated, and f_2 is the portion that depends on factors like external disturbances that are not measurable.

The overall block diagram of the proposed control system is shown as in Fig. 2 below.

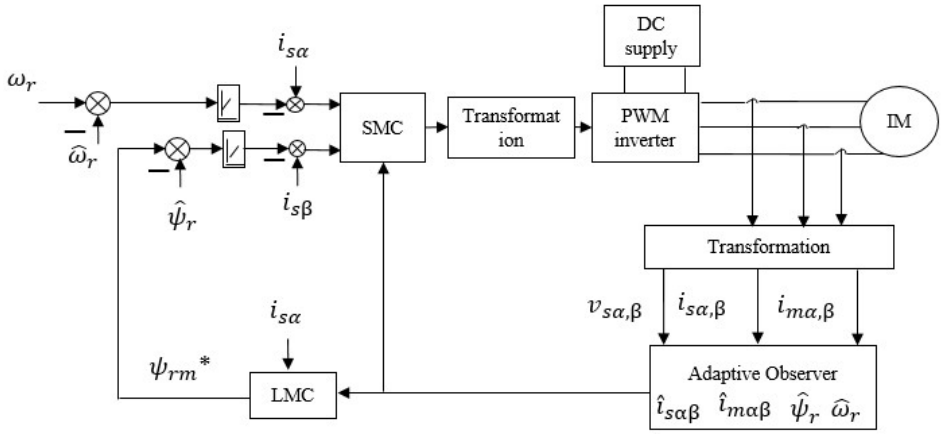

Fig. 2. The schematic diagram of the control structure

3.2. Stability analysis of the proposed system

The observer state-space model, which updates the rotor fluxes and stator currents used for rotor speed adaptation, served as the foundation for the adaptive model's creation. However, the estimator should be in charge of the observation's stability, which may be achieved to the best of its capacity by figuring out the error dynamics and system stability, which were both verified by the Lyapunov stability criterion. This phase demonstrates how the intended algorithm ensures that the switching functions have a zero value.

The estimated rotor speed is tested for stability using the Lyapunov function (V) which is

$$V = \frac{1}{2} s^T s = \frac{1}{2}\left(s_1^2 + s_2^2 + \ldots + s_n^2\right) > 0. \tag{19}$$

If the derivative of the function (19), the system is asymptotically stable.

$$\dot{V} = s^T \dot{s} = s_1\dot{s}_1 + s_2\dot{s}_2 + \ldots + s_n\dot{s}_n \tag{20}$$

is negative.

The observer gains $\boldsymbol{K}$ $(k_1 \ldots k_4)$ are used to have a quick reaction in order to reduce the estimation error and it is obtained from,

$$\det(\boldsymbol{A} - \boldsymbol{K}\boldsymbol{I}) = 0, \tag{21}$$

where $\boldsymbol{A}$ is the system matrix from the transfer function and $\boldsymbol{I}$ is the identity matrix.

The stability analysis is proofed by considering two different cases,

Case 1) $\omega_r = -1, \ldots, 1$, $\lambda\alpha = 5$, $\zeta = 0.4$, $\Psi = 0.2$, $\xi = 1$, $\mu = 0.6$ are design parameters.

Therefore, all of the observer poles have negative values for $\xi = 1$ and $\mu = 0.6$ with changes of the rotor speed from –1 to 1 and $TL = 0.7$ p.u. as shown in Fig. 3. This test demonstrates that the AFO structure is stable.

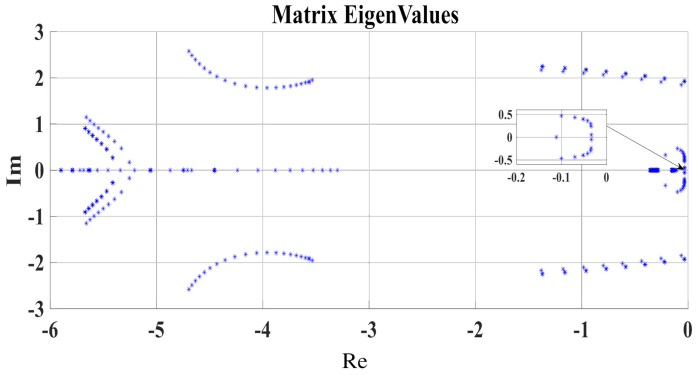

Fig. 3. Spectrum of matrix of the linearized observer system

Case 2) $\omega_r = 1$, $\lambda\alpha = 4$, $\xi = 0.2, \ldots, 1$, $\Psi = 0.2, \ldots, 4$, $\mu = 0.5$.

The spectrum of the linearized observer's matrix is shown in Fig. 4 for constant rotor speed of 1 p.u when ξ changes from 0.2 to 1.0 and $TL = 0.7$ p.u. The poles of the observer structure are all negative values and stable.

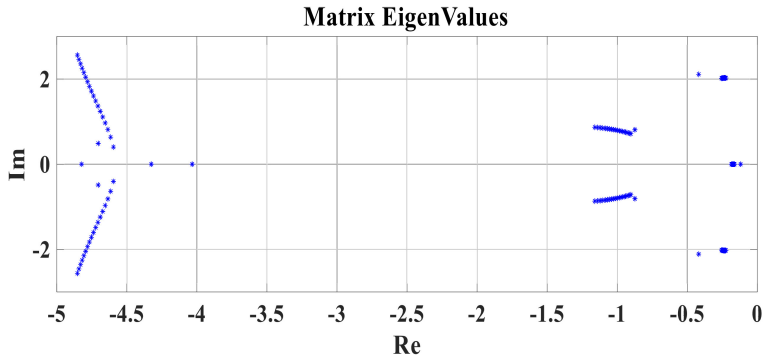

Fig. 4. Spectrum of matrix of the linearized observer system

The observer poles are proportional to the motor poles thanks to the equivalence principle, which specifies that the location of the observer pole is picked by direct comparison. This observer gain is unique due to a term in the equation that subtracts the actual measurement from the estimate of the current output and modifies the current state estimations by a factor corresponding to the prediction error. Even if the system being watched is unstable, this correction ensures the observer's stability and convergence.

4. Loss minimizing function and efficiency calculations of IM

The total power loss of the induction motor is the sum of copper losses, core losses, and mechanical losses. Neglecting the mechanical losses, which are independent of the control mechanism, the total IM loss can be written as [16, 30]

$$\begin{aligned} P_L &= p_L\text{stator} + p_L\text{rotor} + p_L\text{core}, \\ P_L &= 1.5\left(i_{s\alpha}^2 + i_{s\beta}^2\right) + 1.5\left(i_{Rr\alpha}^2 + i_{Rr\beta}^2\right) + 1.5\left(i_{m\alpha}^2 + i_{m\beta}^2\right), \end{aligned} \tag{22}$$

where: $p_L$stator is the stator loss, $p_L$rotor is the rotor loss, $p_L$core is the core or iron loss.

In the loss minimization concept, deriving the relation for the efficiency (η) of an IM is used to determine whether the proposed system is effective or not.

$$\eta = \frac{p_{\text{out}}}{p_{\text{in}}} = \frac{p_{\text{out}}}{p_{\text{out}} + P_L}, \tag{23}$$

where: p_{out} is the motor's useful mechanical output power, p_{in} is the inverter's input power, P_L is the loss power proportional to the motor's internal losses.

It is well known that motor efficiency can be increased by changing the motor fluxes when the load torques are lower than the rated motor torque.

$$P_{Rm} = P_{Rm}(\text{eddy current loss}) + P_{Rm}(\text{hysteresis loss}), \tag{24}$$

$$\begin{aligned} P_{Rm}\,(\text{eddy current loss}) &= k_e\left(\omega^2\psi_{rm}\right), \\ P_{Rm}\,(\text{hysteresis loss}) &= k_h\left(\omega\psi_{rm}\right), \end{aligned} \tag{25}$$

where ω is the stator angular frequency, k_e and k_h are the coefficients of the eddy-current loss and the hysteresis losses, respectively.

Rotor iron loss can be neglected since $|s\omega| \ll |\omega|$ and now the total power loss can be written as

$$P_L = 1.5\left[R_s\left(i_{s\alpha}^2 + i_{s\beta}^2\right) + R_r\left(i_{r\alpha}^2 + i_{r\beta}^2\right)\right] + \omega^2\psi_{rm}/R_m\,. \tag{26}$$

Solving for the rotor currents

$$\begin{aligned} i_{r\alpha} &= \frac{\phi_{r\alpha}}{L_r - L_m} - \frac{L_m i_{m\alpha}}{L_r - L_m}, \\ i_{r\beta} &= \frac{\phi_{r\beta}}{L_r - L_m} - \frac{L_m i_{m\beta}}{L_r - L_m}. \end{aligned} \tag{27}$$

Now writing the square of the stator and rotor currents in (26) as a function of airgap flux and torque the total power loss (P_L) can be written as

$$P_L = \gamma_1\frac{T_e^2}{\psi_{rm}} + \gamma_2\psi_{rm}\,, \tag{28}$$

where: ψ_{rm} is the rotor flux modulus, γ_1 and γ_2 are both calculated to be positive real numbers.

$$\begin{aligned} \psi_{rm} &= \psi_{r\alpha}^2 + \psi_{r\beta}^2\,, \\ \gamma_1 &= \frac{R_s L_r^2 + R_r L_m^2}{L_r^2}, \\ \gamma_2 &= \left(\frac{R_s}{L_m^2}\right) + \left(\frac{\omega^2}{R_m}\right). \end{aligned} \tag{29}$$

When the rotor flux modulus is at a steady state, the loss minimization condition is given by

$$\frac{\partial P_L}{\partial\phi_{r\alpha}} = 0 \quad \text{and} \quad \frac{\partial P_L}{\partial\phi_{r\beta}} = 0. \tag{30}$$

Since P_L is positive definite function, this can be considered as the cost function and then to be minimized with any desired variables which is rotor flux in this case and solution to differential Eq. (28) is the optimum reference flux for loss minimization

$$\psi_{rm}^* = \sqrt{\frac{\gamma_1}{\gamma_2}}\,|T_e|\,. \tag{31}$$

In order to reduce the overall power loss of (28) when the desired value of T_e is provided, loss minimization control algorithm is based on calculating the reference value of ψ_{rm}.

The maximum voltage and current that an induction machine can operate at, as well as the inverter, determine how much developed torque is possible. The machine's and the inverter's voltage ratings are often matched. To give more acceleration torque during transients, the inverter's

current ratings are typically higher than those of the machine [31, 32]. In this work, the voltage ratings of the machine are assumed to be equal to the maximum stator voltage that the inverter can apply to it. Additionally, in order to achieve quick response during the transient duration, the maximum stator current, which is constrained by the inverter current ratings, is considered to be 1.5 times the machine's current ratings:

Next, some calculated parameters will be shown, and the stray losses and windage losses are included in the mechanical losses.

a) Input power

Three-phase IM input power is calculated with and without core resistance (R_m). The input power can be estimated as

$$P_{\text{in}} = \sqrt{3} V_L I_L \cos\theta = 3 V_{\text{ph}} I_{\text{ph}} \cos\theta, \tag{32}$$

where: p_{in} is the input power, V_L is the line voltage, I_L is the line current, V_{ph} is the phase voltage, I_{ph} is the phase current and $\cos\theta$ is the power factor (PF).

b) Air-gap power losses

The stator copper losses are 1.9 kW and the core losses are 1.8 kW and 1.4 kW with and without core resistance respectively. The air-gap power losses can be estimated as [33–35]

$$P_{AG} = P_{\text{in}} - (P_{scL} + P_{\text{core}}), \tag{33}$$

where: P_{AG} is the air gap power, P_{scL} is the stator copper loss, P_{core} is the core loss, P_{conv} is the converted power, P_{RcL} is the rotor copper loss and s is the slip.

c) Converted power losses

To calculate power converted, the only rotor copper losses are 525 W, which is taken into consideration. The converted power losses can be estimated as follows:

$$P_{\text{conv}} = P_{AG} - P_{RcL} = \frac{P_{RcL}}{s} = (1 - s) P_{AG}\,. \tag{34}$$

d) Output power losses

The calculation makes the assumption that stray losses are minimal, thus the friction and windage losses are taken into consideration at 460 W each. The output power losses can be estimated as shown in Table 2.

$$P_{\text{out}} = P_{\text{conv}} - P_{\text{mech}}\,, \tag{35}$$

where P_{out} is the output power and P_{mech} is the mechanical power.

5. Result and discussion

The overall Simulink model of the MRAC-based sliding mode observer was implemented using MATLAB/Simulink software.

As it can be seen from Fig. 5, the developed torque has good starting, and the estimated speed is following the actual speed for a reference speed of 100 rad/s in both the positive and

negative regions. The developed torque settles to zero in very little time and has a smaller harmonic disturbance than that of the controller without the core loss. From the output of torque characteristics, it can be seen that the speed estimator is effective at a very low speed the machine needs maximum torque to achieve the desired speed. Once the motor gets to a desired speed of 100 rad/s, torque becomes zero. Therefore, the proposed controller is robust and has better dynamic performance for induction motors designed with core loss. With a very small amount of overshoot, the estimated speed starts to follow the reference speed, behaving like the actual speed.

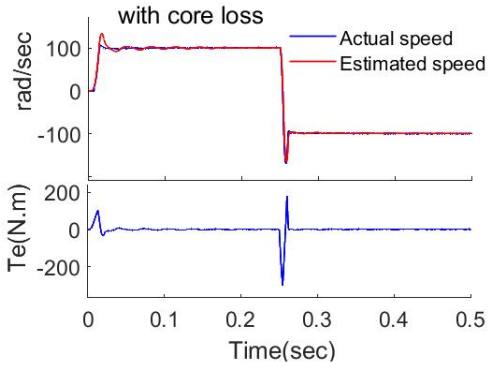

Fig. 5. Induction motor speed response for the proposed controller with core loss

Using the induction motor with the following nominal parameters in Table 1 [13] the verification of the proposed control is done by simulations.

The proposed control system is simulated for forward and backward speed showing better performance close to the reference value for an induction motor modelled with core loss.

Figure 6 shows the AOSMC without core loss-based developed torque, the actual speed, and the estimated speed, respectively. It is possible to see that the advantages of starting torque, good

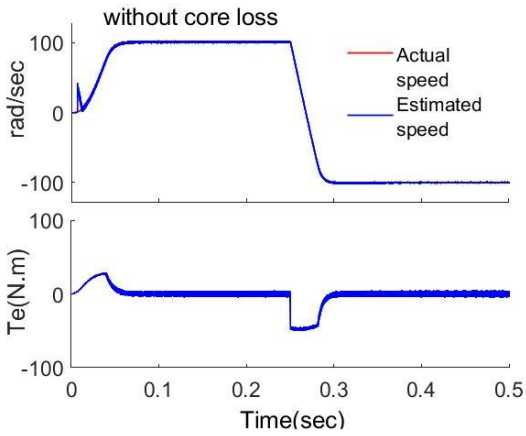

Fig. 6. Induction motor speed response for the proposed controller without core loss

Table 1. IM Parameters and references unit

Quantity	Symbol	Values
Stator resistance	R_s	2.92 Ω
Rotor resistance	R_r	3.36 Ω
Core resistance	R_m	682.59 Ω
Magnetizing inductance	L_m	0.422 H
Stator, rotor inductances	$L_s,\ L_r$	0.439 H
Leakage inductance	L_{ls}	0.017 H
Nominal power	P_n	5.5 kW
Nominal stator voltage	U_n	11 A
Nominal stator current	I_n	400 V
Nominal rotor speed	n	1 430 rpm
Nominal frequency	f	50 Hz
Reference current	$I_b = I_n\sqrt{3}$	19 A
Reference voltage	$U_b = U_n$	400 V
Reference power	P_b	7.6 kW

rising time, and settling time of both the actual speed and estimated speed of the motor with the core loss seen in Fig. 5 above are missed for the one without core loss. From the result, it can be seen that the actual speed and estimated speed started to track the reference speed after 0.06 s, and for the induction motor modelled with core loss, the equivalent is 0.03 s.

a) Simulation result under load variation

In Fig. 7 below, the performance of the proposed system is shown for different loads applied to it. The output is shown for the application of full load torque at no load at 0 s, full load at

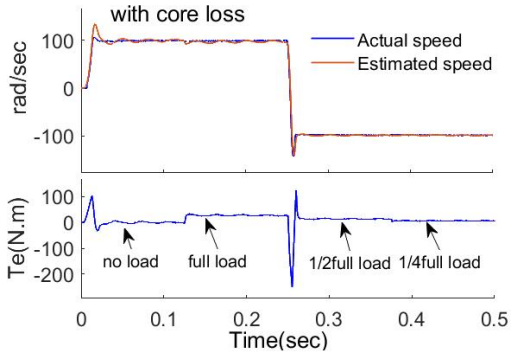

Fig. 7. Simulation result with core loss for different load torques

0.125 s, half of full load torque at 0.25 s, and a quarter of full load torque up to 0.375 s. As can be seen from the result, the system is resisting the applied load torque.

In Fig. 8 below, the performance of the proposed system without core loss is shown for different loads applied to it. The output is shown for the application of full load torque at 0.125 s, half of full load torque at 0.25 s, and a quarter of full load torque at 0.375 s. As it can be seen, the system cannot resist the application of different load torques, unlike ASMOC performance with core loss.

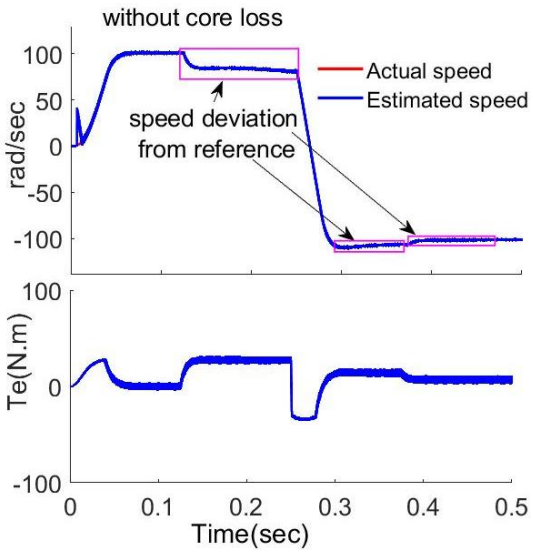

Fig. 8. Simulation result without core loss for different load torques

b) Comparison of the proposed controller results

The performance of an AOSMC induction motor modelled with and without core loss has been shown in Fig. 9 below. The AOSMC without iron loss has less overshoot than that with iron loss, but it takes more rising time, about 0.05 s, and the output signal is distorted and affected by ripple torque. The performance of the controller with iron loss is smooth after a very small overshoot compared to the one without iron loss for the whole range of simulation time.

In Fig. 10 below, the comparison is shown by applying full load torque at 0.125 s, half of full load torque at 0.25 s, and a quarter of full load torque up to 0.375 s.

The speed error of AOSMC induction motor control with and without core loss is shown in Fig. 11 as compared to the 100 rad/s of the reference speed. From the error output, it can be seen that the speed error of the AOSM controller without iron loss becomes zero at 0.01 s, and after 0.012 s, the error is greater than zero due to load variation, but the error is below 2%, so it is an unacceptable error. The output error of the AOSMC with core loss is zero after 0.02 s and almost goes away with time in seconds. The output error of the AOSMC gives a guarantee for the stability of the overall system.

The rotor fluxes and stator currents are shown as in Fig. 12(a) and 12(b) below, respectively.

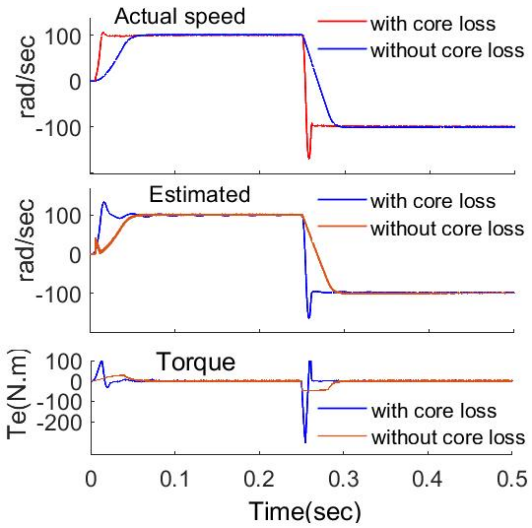

Fig. 9. Torque, actual and estimated speed response comparison with and without core loss

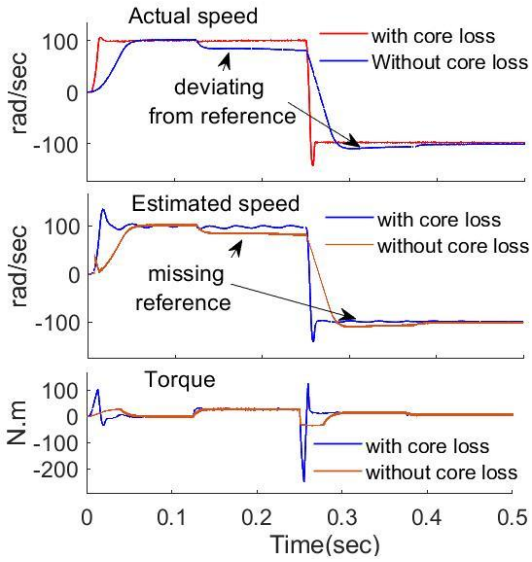

Fig. 10. Torque, actual and estimated speed response comparison with and without core loss under different load conditions

As can be seen from Fig. 13 below in high-performance drives, the adjustable-speed controller's primary function is to follow the reference speed as quickly as feasible, and operating induction motors with less flux at light loads will minimize energy consumption.

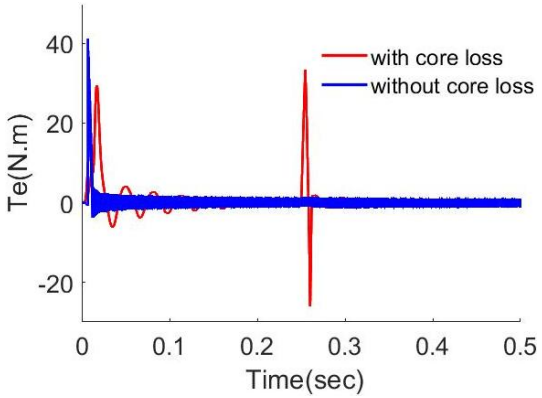

Fig. 11. Speed error comparison with and without core loss

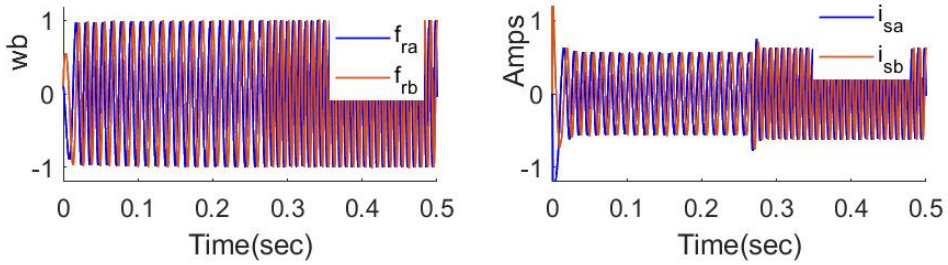

(a) (b)

Fig. 12. Rotor fluxes (a); stator currents (b)

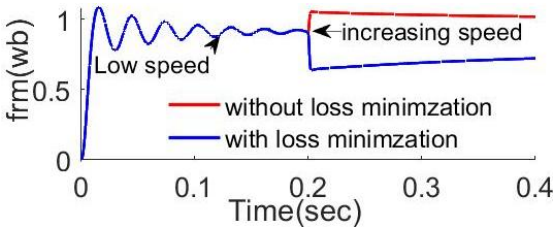

Fig. 13. Comparison of required fluxes with and without loss minimization

Therefore, the reference value of growth to the nominal level might be implemented with respect to system boundaries when the step speed command increase comes at a low load and flux level.

Table 2 shows the calculated efficiency with and without core resistance of the IM drive, and by comparison, the results obtained with core resistance are greater than those obtained without core resistance.

Table 2. Calculated power losses and efficiency of IM drive with and without Rm

Measurements	IM modelled with Rm	IM modelled without Rm	Unit
Stator copper loss (P_{scL})	0.525	1.9	kW
Rotor copper loss (P_{RcL})	0.525	0.525	kW
Core loss	1.6	1.4	kW
Mechanical loss (P_{mech})	0.460	0.460	kW
Input power (P_{in})	17	15.875	kW
Converted power loss (P_{conv})	14.075	16.4	kW
Output power (P_{out})	19.54	13.615	kW
Efficiency	0.87	0.85	%

6. Conclusion

The performance of the proposed sensorless speed estimation control for IMs has been analysed. The rotor speed estimation is done using estimated rotor fluxes and stator currents from the adaptive observer. The simulation results show the good dynamic performance and robustness of the AOSMC. The proposed system is tested by considering different operating conditions, such as no-load, variable load torque, low and higher speed ranges, and varying the rotor inductance and resistance value. The controller shows better performance for IMs with core loss than the one without core loss. The proposed system has a good rising time, and it settles better for IMs with core loss than the one without core loss. The SMC part of the torque component current estimator shows a low chattering effect on the sliding surface for torque production. This ensures stability and reduces the effects of parameter variation and ripple torque. Therefore, the proposed estimation is robust and achieves good characteristics for sensorless control of IMs with core loss.

References

[1] Rouabah Z., Abdelhadi B., Anayi F., Zidani F., *On-line losses minimization of induction motor vector control*, Archives of Electrical Engineering, vol. 60, no. 3, pp. 257–268 (2011), DOI: 10.2478/v10171-011-0024-5.

[2] Ryszard B., *Estimation of parameters of selected converter drives*, Archives of Electrical Engineering, vol. 61, no. 4, pp. 533–565 (2012), DOI: 10.2478/v10171-012-0041-z.

[3] Wogi L., Ayana T., Morawiec M., Andrzej J., *A Comparative Study of Fuzzy SMC with Adaptive Fuzzy PID for Sensorless Speed Control of Six-Phase Induction Motor*, Energies, vol. 15, no. 8183, pp. 1–29 (2022), DOI: 10.3390/en15218183.

[4] Wogi L., Thelkar A., Tahiro T., Ayana T., Urooj S., Larguech S., *Particle Swarm Optimization Based Optimal Design of Six-Phase Induction Motor for Electric Propulsion of Submarines*, Energies, vol. 15, no. 2994, pp. 1–21 (2022), DOI: 10.3390/en15092994.

[5] Quan N., Tam N., Nho N., Nghia D., *Sliding Mode Control of a Three Phase Induction Motor Based on Reference Model*, International Conf. on System Science and Engineering (ICSSE), Ho Chi Minh City, Vietnam, pp. 702–716 (2017), DOI: 10.1109/ICSSE.2017.8030968.

[6] Mohanty K., *Sensorless sliding mode control of induction motor drives*, TENCON 2008 - 2008 IEEE Region 10 Conference, Hyderabad, India, pp. 1–6 (2008), DOI: 10.1109/TENCON.2008.4766709.

[7] Colin S., *Adaptive speed identification for vector control of induction motors without rotational transducers*, IEEE Transactions on Industry Applications, vol. 28, no. 5, pp. 1054–1061 (1992), DOI: 10.1109/28.158829.

[8] Bazzi A., Krein P., *Review of methods for real-time loss minimization in induction machines*, IEEE Transactions on Industry Applications, vol. 46, no. 6, pp. 2319–2328 (2010), DOI: 10.1109/TIA.2010.2070475.

[9] Liu X., Yu H., *Continuous adaptive integral-type sliding mode control based on disturbance observer for PMSM drives*, Springer Nature, vol. 34, no. 104, pp. 1429–1441 (2021), DOI: 10.1007/s11071-021-06360-z.

[10] Wenxin Y., Shao Dao H., Dan J., *A fault monitoring method for wind power generation system based on sliding mode observer*, Archives of Electrical Engineering, vol. 67, no. 3, pp. 625–643 (2020), DOI: 10.24425/aee.2020.133922.

[11] Navaneethan S., Kanthalakshmi S., Aandrew B.S., *Lyapunov stability based sliding mode observer for sensorless control of PMSM*, Bull. of The Polish Academy of Sciences Technical Sciences, vol. 70, no. 2, pp. 1–8 (2022), DOI: 10.24425/bpasts.2022.140353.

[12] Mahdi S., Alireza S., Vahab N., Cristian G., Jose R., *Integral Sliding Mode Observer-Based Ultra local Model for Finite-Set Model Predictive Current Control of Induction Motor*, IEEE Journal of Emerging and Selected Topics in Power Electronics, vol. 10, no. 3, pp. 2912–2922 (2022), DOI: 10.1109/JESTPE.2021.3110797.

[13] Morawiec M., Lewicki A., *Application of Sliding Switching Functions in Backstepping Based Speed Observer of Induction Machine*, IEEE Transactions on Industrial Electronics, vol. 67, no. 7, pp. 5843–5853 (2020), DOI: 10.1109/TIE.2019.2914645.

[14] Maamouri R., Trabelsi M., Boussak M., M'Sahli F., *Second-order SMO-based sensorless control of IM drive: experimental investigations of observer sensitivity and system reconfiguration in post fault operation mode*, IET Electric Power Applications, vol. 15, no. 1, pp. 811–823 (2020), DOI: 10.1049/elp2.12057.

[15] Bartolini G., Punta E., Zolezzi T., *First and Second Order Slide Mode Regularization Techniques: The Approximability Property*, Elseiver 16th Triennial World Congress, Prague, Czech Republic, pp. 878–882 (2005), DOI: 10.3182/20050703-6-CZ-1902.00802.

[16] Di Gennaro S., Rivera J., Meza M., *Sensorless High Order Sliding Mode Control of Induction Motors With Core Loss*, IEEE Transactions on Industrial Electronics, vol. 61, no. 6, pp. 2678–2689 (2014), DOI: 10.1109/TIE.2013.2276311.

[17] Zhao Y., Yu H., Wang S., *An Improved Super-Twisting High-Order Sliding Mode Ob-server for Sensorless Control of Permanent Magnet Synchronous Motor*, Energies, vol. 14, no. 6047, pp. 1–18 (2021), DOI: 10.3390/en14196047.

[18] Horch M., Boumediene A., Baghli L., *Sensorless High-order Super Twisting Sliding Modes Vector Control for Induction Motor Drives*, 8th International Conference on Modelling, Identification and Control, Algiers, Algeria, pp. 237–2442 (2016), DOI: 10.1109/ICMIC.2016.7804115.

[19] Salah E., Djamel S., Noureddine G., *High-performance induction motor drive based on adaptive super-twisting sliding mode control approach*, Archives of Electrical Engineering, vol. 71, no. 1, pp. 245–263 (2022), DOI: 10.24425/aee.2022.140208.

[20] Djilali K., Mohamed T., Mohamed S., *Improved direct torque control of induction motors using adaptive observer and sliding mode control*, Archives of Control Sciences, vol. 23, no. 3, pp. 361–376 (2013), DOI: 10.2478/acsc-2013-0022.

[21] Johnson B., Willis J., *Tailoring induction motor analytical models to fit known motor performance characteristics and satisfy particular study needs*, IEEE Transactions on Power Systems, vol. 6, no. 3, pp. 959–965 (1991), DOI: 10.1109/59.119235.

[22] Leedy A., *Simulink/MATLAB Dynamic Induction Motor Model for use in Undergraduate Electric Machines and Power Electronics Courses*, 2013 Proceedings of IEEE SoutheastCon, Jacksonville, FL, USA, pp. 1–6 (2013), DOI: 10.1109/SECON.2013.6567399.

[23] Kirschen D., Novotny D., Lipo T., *On-line efficiency optimization of a variable frequency induction motor drive*, IEEE Trans. on Industrial Application, vol. 21, pp. 610–615 (1985), DOI: 10.1109/TIA.1985.349717.

[24] Chakraborty C., Hori Y., *Fast Efficiency Optimization Techniques for the Indirect Vector-Controlled Induction Motor Drives*, IEEE Transactions on Industry Applications, vol. 39, no. 4, pp. 1070–1076 (2003), DOI: 10.1109/TIA.2003.814550.

[25] Fernández-Bernal F., Garcia-Cerrada A., Faure R., *Model-Based Loss Minimization for DC and AC Vector-Controlled Motors Including Core Saturation*, IEEE Transactions on Industry Applications, vol. 36, no. 3, pp. 755–763 (2000), DOI: 10.1109/28.845050.

[26] Guo Z., Zihang Q., *The Study on Mathematical Model and Simulation of Asynchronous Motor Considering Iron Loss*, Journal of Physics: Conference Series, Shanghai, China, pp. 1–7 (2018), DOI: 10.1088/1742-6596/1060/1/012085.

[27] Ibtissem B., Souad Ch., Abdesselam M., *High performance backstepping control of induction motor with adaptive sliding mode observer*, Archives of Control Sciences, vol. 21, no. 3, pp. 331–344 (2011), DOI: 10.2478/v10170-010-0047-y.

[28] Dunnigan M., Wade S., Williams B., Yu X., *Position control of a vector controlled induction machine using Slotine's sliding mode control approach*, IEE Proceedings - Electric Power Applications, vol. 145, no. 3, pp. 231–238 (1998), DOI: 10.1177/014233120102300202.

[29] Orlowska-Kowalska T., Tarchala G., *Unified approach to the sliding-mode control and state estimation*, Bull. of the Polish Academy of Sciences, Technical Sciences, vol. 61, no. 4, pp. 837–846 (2013), DOI: 10.2478/bpasts-2013-0090.

[30] Adamowicz M., GuzińskiJ., *Minimum-time minimum-loss speed sensorless control of induction motors under nonlinear control*, conf. paper in IEEE Compatibility in Power Electronics, Gdynia, Poland, pp. 1–7 (2015). DOI: 10.1109/CPE.2005.1547546" 10.1109/CPE.2005.1547546.

[31] Chang J., Kim B., *Minimum-Time Minimum-Loss Speed Control of Induction Motors Under Field-Oriented Control*, IEEE Transactions on Industrial Electronics, vol. 44, no. 6, pp. 809–815 (1997), DOI: 10.1109/41.649942.

[32] Xu X., Novotny D., *Selecting the flux reference for induction machine drives in the field weakening region*, IEEE Transactions on Industry Applications, vol. 28, pp. 1353–1358 (1992), DOI: 10.1109/IAS.1991.178180.

[33] Kassem R., Sayed K., Kassem A., Mostafa R., *Power optimization scheme of induction motor using FLC for electric vehicle*, IET Electrical Systems in Transportation, vol. 10, no. 3, pp. 301–309 (2020), DOI: 10.1049/iet-est.2019.0151.

[34] Sahoo A., Jena R., *Loss minimization of induction motor-driven electric vehicle using teamwork optimization*, International Journal of Ambient Energy, vol. 43, no. 1, pp. 8123–8134 (2022), DOI: 10.1080/01430750.2022.2091036.

[35] Sayed K., El-Zohri E., Mahfouz H., *Analysis and design for interleaved ZCS buck DC-DC converter with low switching losses*, International Journal of Power Electronics, vol. 8, no. 3, pp. 210–231 (2017), DOI: 10.1504/IJPELEC.2017.085076.